

Design of Variable Frequency Control System of Direct-drive Wind Motor

LIU Quan ^{*1}, HUANG Zhengjun ^{*2}, ZHANG Yibo ^{*3}

^{*1} Beijing Information Science and Technology University, No. 12, Qinghe Xiaoying East Road, Haidian District, Beijing
E-mail: Liuq16@163.com

^{*2} Beijing Information Science and Technology University, No. 12, Qinghe Xiaoying East Road, Haidian District, Beijing
E-mail:2582538909@qq.com

^{*3} Beijing Information Science and Technology University, No. 12, Qinghe Xiaoying East Road, Haidian District, Beijing

Abstract. Based on the analysis of the principle and traditional control strategy of the converter, according to the design requirements of the converters, the design of the machine-side converter and the grid-side converter is introduced in detail. The converter control adopts zero DC current control and speed outer loop current inner loop control mode, and the grid-side converter adopts voltage outer loop current inner loop control control strategy. It provides a theoretical basis for the subsequent establishment of the converter simulation model.

Keywords: Wind Turbine, Direct Drive, Pitch Controller, Variable Frequency Control

1. INTRODUCTION (HEADING 1)

Permanent magnet direct drive type wind turbine is a multi-pole generator directly driven by the wind wheel shaft to generate electricity. Compared with doubly-fed wind turbine, the transmission chain is simplified, and the low-speed shaft, high-speed shaft, coupling and gear box are eliminated. , The length of the nacelle is reduced, the structure is more compact, and the problem of regular replacement of gear box oil and economic losses caused by gear box failure is avoided, maintenance costs are reduced, and transmission loss of the gear box is reduced. It has the advantages of high power generation efficiency. In recent years, with the development of mobile robot technology, motor control has become the core problem [1-10]. The permanent magnet direct drive wind turbine control system mainly includes four components: the main controller, the pitch controller, the yaw controller, and the converter controller [11]. Among them, the converter completes the variable-speed and constant-frequency control of the generator, ensures the quality of power generation and grid connection, and achieves the same frequency, amplitude, and phase with the grid voltage; when the wind speed is less than the rated wind speed and when the blade pitch angle of the wind turbine remains the most When hours, the converter controls the generator speed and electromagnetic torque to maintain the optimal blade tip rotation speed ratio for high-speed operation. When the wind speed driving the rotation of the wind wheel exceeds the rated power generation wind speed, the pitch controller is used to

limit the power and reduce the power grid. Voltage and power fluctuations [12-14].

The converter of a large-scale direct-drive wind motor is a key component that connects the generator and the power grid. It turns the alternating current generated by the generator into alternating current that meets the power frequency requirements of the power grid and controls the speed and torque of the generator at the same time, To achieve the power factor adjustment of the power generation system and reduce the grid-connected harmonic current components [15], so the design of the converter control system is the key and difficult point of the direct drive wind power technology.

At present, there are relatively few documents on the design technology of direct drive wind power converter control system [16], but the main control strategy is only the generator-side converter to realize the decoupling control of the reactive and active power of the permanent magnet synchronous generator. The voltage control of the DC side and the grid-connected output are realized by the grid-side converter [17]. However, there are also some literatures that propose different methods: Ref [18] proposes a strategy for connecting energy dissipation resistors to the DC bus. In [19] a cross-coupling design between the grid-side converter and the machine-side converter is proposed. The method of the controller, ref [20] proposes a control method using dual PWM full power converters and space vector. Ref [21] proposes a strategy for coordinated control using AC and DC power grids. Ref [22] proposes the use of fixed Voltage control method. In [23], a control method using voltage frequency is proposed. However, these methods have problems such as the instability of the output power of the DC grid due to the indirect power supply. Foreign research on direct drive wind turbines mainly focuses on converter control algorithms, direct drive wind turbine converter modeling, and how to improve the ability of the converter to ride through faults [24].

In response to the above problems, this paper analyzes the principle of the converter and traditional control strategies, and according to the design requirements of the converter, designs the machine-side converter and the grid-side converter. The converter control adopts zero DC Current control and speed outer loop current inner loop control mode, the grid-side converter adopts the voltage outer loop current inner loop control strategy, the

converter simulation model is established, and the Simulink tool of Matlab is used to analyze the direct drive wind motor's machine side and The grid-side converter is simulated and analyzed.

2. DESIGN OF GENERATOR-SIDE CONVERTER CONTROLLER

The generator-side converter of the direct-drive wind turbine generator needs to change the alternating current output by the permanent magnet generator stator into direct current. When the unit is running at the rated wind speed, the generator-side converter controls the generator speed to achieve the optimal blade tip The speed ratio captures the maximum wind energy.

The maximum torque/current control strategy of the machine-side converter is adopted, that is, the zero d-axis current control strategy. The current loop adopts PI adjustment. In order to achieve the maximum power control and capture the maximum wind energy, at the rated wind speed, the motor reference speed is calculated according to the output power value and wind speed of the grid-side converter, and it is compared with the actual speed of the generator to obtain the speed error. The reference current is obtained by the PI regulator of the outer speed loop, and the dq axis voltage is obtained by the difference between the reference current and the actual current via the PI regulator of the current loop. The voltage undergoes coordinate transformation and PWM modulation to obtain a specific switching sequence for the grid-side switching devices of the converter. The output voltage tracking speed control realizes the maximum power tracking control, and the d-axis reference current of the generator-side converter is kept constant at zero.

If p_r is the power generated by the permanent magnet generator, after the power is rectified by the generator-side converter, the AC output from the stator side of the generator becomes DC. The grid-side converter adjusts the DC bus voltage value to become amplitude, The frequency and phase meet the requirements of the power frequency grid to obtain AC power. p_l is the power output from the grid-side converter to the grid.

The current I flowing through the capacitor C on the DC side is:

$$i_c = C \frac{dU_{dc}}{dt} = i_{dc} - i_L \quad (1)$$

The outgoing electric power of the PMW converter on the machine side is:

$$P_R = U_{dc} i_{dc} \quad (2)$$

Power absorbed by grid-side converter:

$$P_l = U_{dc} i_L \quad (3)$$

If $P_R = P_l$, U_{dc} is a constant value, and it needs to be closed-loop controlled.

The capacitance does not exceed its upper limit when

achieving better voltage following:

$$C \leq \frac{t_r^*}{0.74R_L} \quad (4)$$

In the formula, t_r is the capacitor charging time, i_r is the equivalent DC load, and i_r^* is the relative value of the maximum value of the DC voltage dynamic drop.

3. DESIGN OF GRID-SIDE CONVERTER

Grid-side converter control is based on unit power factor control to run the converter and perform reactive power compensation in the event of a grid failure. It is also necessary to design the LC AC side filter circuit to achieve the grid-connected harmonic requirements. In order to achieve the DC bus voltage stability goal, the voltage outer loop and current inner loop control strategies are adopted for dual closed-loop control, and the current inner loop requires synchronous grid connection.

3.1. Control Design of Current Loop

The grid-side converter is to control the current input to the grid-side converter and convert the direct current into alternating current that meets the grid-connected requirements. Effective and real-time control of the input current is the key to improving the efficiency of energy flow.

In the coordinate axis component of the two-phase synchronous rotating coordinate system after the dq coordinate transformation, the magnitude of the d-axis current i_{gd} and the q-axis current i_{gq} are determined by the magnitude of the d-axis voltage u_{gd} , the axis current and the coupled phase voltage. In order to reduce the difficulty of its design, Laplace transform is performed on the formula.

According to the symmetry of the d and q -axis currents, the design methods of the two current devices are the same. Therefore, only the design of the d -axis current controller is analyzed here. With i_{gd} as the controlled object and u_{gd} as the output of the controller, a closed-loop control system can be obtained. Block diagram, as shown in Fig. 1

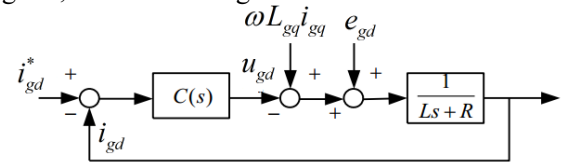


Fig. 1 Block diagram of current inner loop closed loop control motor

According to the control block diagram of the current inner loop in Fig 1, the transfer function can be obtained as follows

$$u_{gd} = C(s)(i_{gd}^* - i_{gd}) \quad (5)$$

The d-axis current i_{gd} is jointly determined by the

reference current i_{gd}^* , the q-axis current i_{gq} and the grid voltage vector d-axis component e_{gd} . The decoupling control method is used to cancel the coupling term, so that it is not affected by i_{gq} and e_{gd} .

The control equation of the AC side voltage is:

$$u_{gd} = -C(s)(i_{gd}^* - i_{gd}) + \omega L_{gq} i_{gq} + e_{gq} \quad (6)$$

Simplify Fig 1 to get:

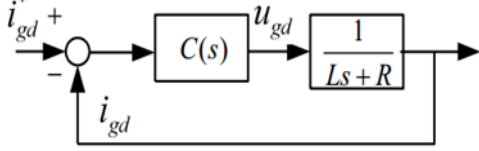


Fig. 2 Block diagram of current inner loop control after decoupling.

The PI control zero is offset to the pole of the current inner loop control. When $\tau_i = \frac{L}{R}$, the transfer function becomes:

$$W_{oi}(s) = \frac{K_{ip} K_{PWM}}{R\tau_i s (1.5T_s s + 1)} \quad (7)$$

The simplified transfer function of the current inner loop is a first-order system:

$$W_{ci}(s) = \frac{1}{3T_s s + 1} \quad (8)$$

The inertial time system is $3T_s$, and the frequency bandwidth f_{bi} of the closed-loop system:

$$f_{bi} = \frac{1}{2\pi(3T_s)} = \frac{1}{6\pi T_s} = \frac{1}{20} f_s \quad (9)$$

In the formula, f_s is the switching frequency of the PWM rectifier and it can well suppress the frequency noise of the switching device.

3.2. Design of voltage outer loop controller

When designing the voltage outer loop control, it is necessary to determine the conversion coefficients from DC current i_{dc} to AC current i_{gd} and i_{gq} as follows:

$$i_{dc} = \frac{3}{2} (S_{gd} i_{gd} + S_{gq} i_{gq}) \quad (10)$$

S_{gd} and S_{gq} are the components of the switching function of the switching device of the grid-side converter on the dq axis respectively. When the converter is operating at high frequency, it is approximately unit power control operation. After stabilization, $i_{gd} = 0$, the relation of the DC and AC d-axis are obtained.:

$$i_{dc} = \frac{3}{2} S_{gd} i_{gd} \quad (11)$$

Simplified to the maximum gain of the proportional link, since the instantaneous power of the grid-side converter is: $P_l = U_{dc} i_L$, the analysis of the voltage outer loop control is similar to the design of the i_{gd} current inner loop, and the inductor resistance is small, so S_{gd} is the representation of Maximum under empty load conditions.

When the switching period and sampling time are very small, the voltage outer loop control is shown in Fig.3.

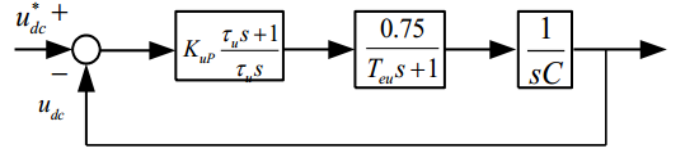


Fig. 3 Combining time constant voltage outer loop control block diagram

When designing the voltage outer loop control, it is necessary to consider that the system has good immunity. After using the classic II system concept for the design, the voltage outer loop open loop transfer function is as follows:

$$W_{ou}(s) = \frac{0.75 K_{up} (\tau_u s + 1)}{C \tau_u s^2 (T_{eu} s + 1)} \quad (12)$$

The frequency bandwidth of the available voltage outer loop is:

$$h_u = \frac{\tau_u}{T_{eu}} \quad (13)$$

The cut-off frequency of the voltage outer loop is:

$$\omega_c = \frac{3}{20T_s} \quad (14)$$

The frequency bandwidth of the voltage outer loop control system is:

$$f_{bu} \approx \frac{\omega_c}{2\pi} = \frac{3}{20T_s \cdot 2\pi} \approx 0.024 f_s \quad (15)$$

4. SIMULATION ANALYSIS OF THE GENERATOR-SIDE AND GRID-SIDE CONVERTERS OF A DIRECT-DRIVE WIND TURBINE

The model established in the simulink platform is that the grid-side converter's DC bus voltage setting is maintained at 710V, the output AC current RMS is 220V, and it is incorporated into the 110KV grid. The DC link capacitance is 4.2MF, the inductance is 0.026Mh, and the filter capacitor is 0.0013MF. The switching devices in the generator-side and grid-side converters are insulated gate bipolar transistors, and phase lockers are used to

obtain the grid voltage frequency and phase for phase measurement.

When the system is running, it can be known that the three-phase current waveform sine wave meets the design goal. Wind speed changes, the stator q-axis current jumps significantly, and the response is good, and the d-axis stator current component remains zero. Fig. 4 is a three-phase stator current waveform diagram. Fig. 5 is a waveform diagram of the stator three-phase current change. At $t=1s$, the current amplitude changes significantly. The three-phase AC output by the grid-side converter is basically stable at 50Hz, and the three-phase voltage waveform is a symmetrical sine wave. Fig. 6 shows the voltage amplitude of 318V, which is equivalent to 220V, which meets the grid design requirements.

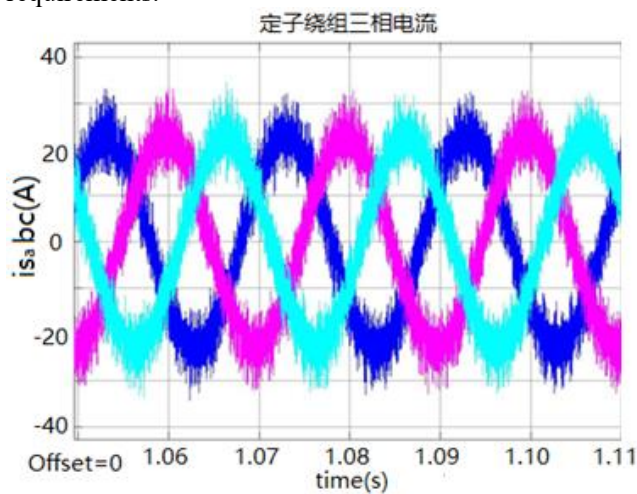


Fig. 4 Three-phase stator current waveform diagram

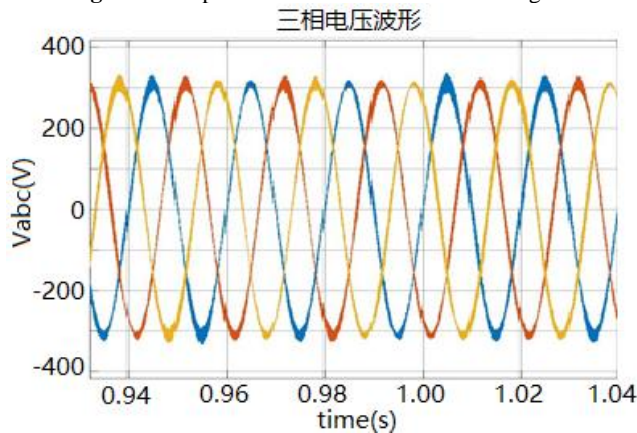


Fig. 5 Waveform diagram of stator three-phase current change

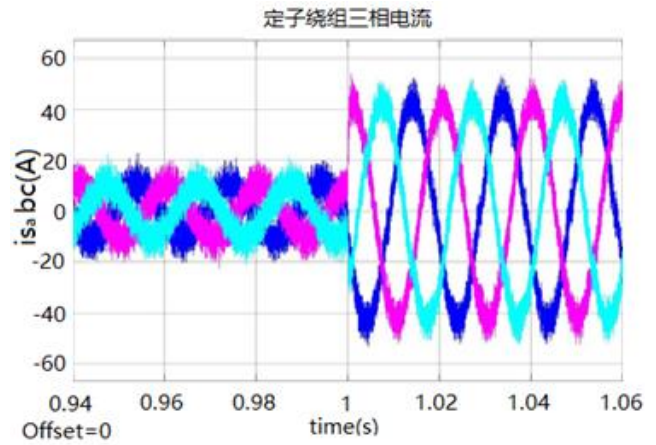


Fig. 6 Grid-side three-phase voltage waveform diagram

5. Conclusion

On the basis of explaining the principle and traditional control strategy of the converter, according to the design requirements of the machine-side and grid-side converters, the machine-side converter and the grid-side converter are designed in detail, and the machine-side converter is controlled. Using zero DC current control and speed outer loop current inner loop control, the grid-side converter adopts voltage outer loop current inner loop control strategy, and MATLAB/Simulink software is used to simulate and analyze large-scale direct-drive wind turbines, which proves the converter The effectiveness of the controller design, and the simulation analysis of the unit under complex wind conditions, verify that the design of the pitch and variable frequency controller has strong adaptability.

REFERENCES:

- [1] Chen Z, Wang S, Wang J, et al. Control strategy of stable walking for a hexapod wheel-legged robot[J]. ISA transactions, 2021, 108: 367-380.
- [2] Li J, Qin H, Wang J, et al. OpenStreetMap-based autonomous navigation for the four wheel-legged robot via 3D-Lidar and CCD camera[J]. IEEE Transactions on Industrial Electronics, 2021.
- [3] Li J, Wu Q, Wang J, et al. Neural networks - based sliding mode tracking control for the four wheel - legged robot under uncertain interaction[J]. International Journal of Robust and Nonlinear Control, 2021, 31(9): 4306-4323.
- [4] Chen Z, Li J, Wang J, et al. Towards Hybrid Gait Obstacle Avoidance for a Six Wheel-Legged Robot with Payload Transportation[J]. Journal of Intelligent & Robotic Systems, 2021, 102(3): 1-21.
- [5] Li, J., Wang, J., Wang, S., Peng, H., Wang, B., Qi, W., Zhang, L., and Su, H. "Parallel structure of six wheel-legged robot trajectory tracking control with heavy payload under uncertain physical interaction", Assembly Automation, 2020, 40(5), 675-687.
- [6] Li J, Wang J, Peng H, et al. Fuzzy-torque approximation-enhanced sliding mode control for lateral stability of mobile robot[J]. IEEE Transactions on Systems, Man, and Cybernetics: Systems, 2021.
- [7] Li J, Wang S, Wang J, et al. Iterative learning control for a distributed cloud robot with payload delivery[J]. Assembly Automation, 2021.

- [8] Li J, Wang J, Peng H, et al. Neural fuzzy approximation enhanced autonomous tracking control of the wheel-legged robot under uncertain physical interaction[J]. *Neurocomputing*, 2020, 410: 342-353.
- [9] Wang, S., Chen, Z., Li, J., and Wang, J.(2021), "Flexible Motion Framework of the Six Wheel-legged Robot: Experimental Results", *IEEE/ASME Transactions on Mechatronics*, 2021, doi: 10.1109/TMECH.2021.3100879.
- [10] Chen Z, Wang S, Wang J, et al. Attitude stability Control for Multi-Agent Six Wheel-Legged Robot[J]. *IFAC-PapersOnLine*, 2020, 53(2): 9636-9641.
- [11] Zhang Yibo. Research on pitch and variable frequency control of direct-drive wind turbines[D]. Beijing Information Science and Technology University, 2020.
- [12] Xiao Wenjuan. Simulation research on grid-side converter control strategy of direct drive wind power system[D]. Lanzhou University of Technology, 2012.
- [13] Youjie Ma, Xia Yang, Xuesong Zhou, Luyong Yang, Yongliang Zhou. Dual Closed-Loop Line ar Active Disturbance Rejection Control of Grid-Side Converter of Permanent Magnet Direct-Drive Wind Turbine[J]. *MDPI*, 2020, 13(5).
- [14] Yan Xiangwu, Li Junyan, Wei Xing. Research on the control strategy of direct-drive permanent magnet synchronous wind turbines in the full wind speed range[J]. *Power System Protection and Control*, 2019, 47(23): 138-144.
- [15] Li Guanghui, Wang Weisheng, Liu Chun, Jin Yiding, He Guoqing. Broadband oscillation mechanism and suppression method of direct drive wind farm connected to weak grid: analysis of broadband impedance characteristics and oscillation mechanism[J]. *Proceedings of the Chinese Society of Electrical Engineering*, 2019, 39(22): 6547-6562.
- [16] Zheng Xinyu, Sun Shiyun, Zhang Xuejuan, Wang Chunyou, Zhao Wei. Influence of grid-connected direct drive wind farm on system static voltage stability[J]. *Electric Machines and Control Applications*, 2019, 46(10): 25-34 +45.
- [17] Huang Hua, Lu Yuye, Pan Xueping, Yuan Xiaoming, Jin Yuqing, Ju Ping. Equivalent modeling of direct drive permanent magnet wind farm based on the operating time of the limiter link[J]. *Journal of Hohai University (Natural Science Edition)*, 2019, 47(01): 88-94.
- [18] Zhang Xianping. Research on low voltage ride-through of direct-drive variable-speed constant-frequency wind power generation system[J]. *High-power converter technology*, 2010(4): 28-31.
- [19] Hansen A D, Michalke G. Multi-pole permanent magnet synchronous generator wind turbines' grid support capability in uninterrupted operation during grid faults [J]. *IET Renewable Power Generation*, 2009, 3(3): 333 — 348
- [20] Liu Jingli, Zhang Youpeng, Gao Fengyang, Dong Weiguang. Control strategy and simulation study of permanent magnet direct drive wind power converter[J]. *Power Technology*, 2012, 36(04): 554-557.
- [21] Liu X, Wang P M, Loh P C. A hybrid AC/DC microgrid and its coordination control[J]. *IEEE Trans on smart Grid*, 2011, 2(2): 278-286.
- [22] Akbari M, Golkar M A, Tafreshi S M M. Voltage control of a hybrid AC/DC microgrid in grid-connected operation mode [C]// *Proceedings of IEEE Conference PES Innovative Smart Grid Technologies, Kollat, India, 2011*.
- [23] Akbari M, Golkar M A, Tafreshi S M M. Firefly algorithm-based voltage and frequency control of a hybrid AC-DC microgrid [C]// *Proceedings of IEEE Conference Electrical Power Distribution Networks, Tehran, Iran, 2012*.
- [24] Tang Lei, Zeng Chengbi, Miao Hong, Xu Wei, Yang Yan. New control strategy of AC/DC bidirectional power converter in AC/DC hybrid microgrid[J]. *Power System Protection and Control*, 2013, 41(14): 13-18.